ROYAL SOCIETY OF CHEMISTRY

Lab on a Chip

General defocusing particle tracking

Journal:	*Lab on a Chip*
Manuscript ID:	LC-MET-05-2015-000562.R1
Article Type:	Paper
Date Submitted by the Author:	29-Jun-2015
Complete List of Authors:	Barnkob, Rune; Bundeswehr University Munich, Institute of Fluid Mechanics and Aerodynamics Kaehler, Christian; Bundeswehr University Munich, Institute of Fluid Mechanics and Aerodynamics Rossi, Massimiliano; Bundeswehr University Munich, Institute of Fluid Mechanics and Aerodynamics

SCHOLARONE™
Manuscripts
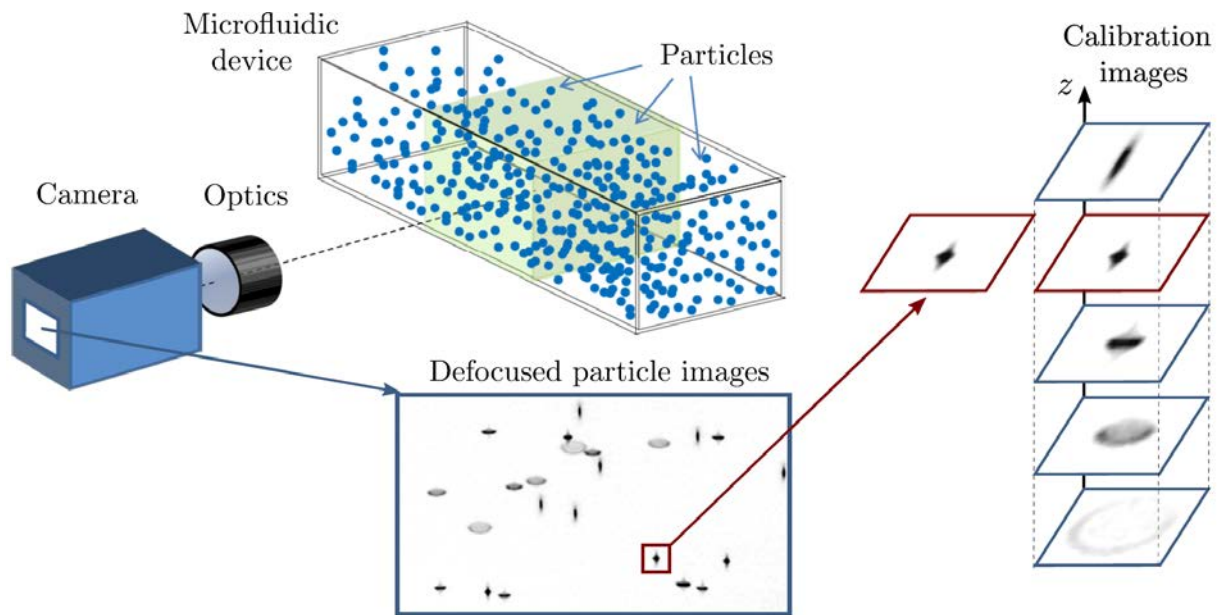
The General Defocusing Particle Tracking (GDPT) is a 3D particle tracking method that relies on a simple empirical procedure based on a calibration image stack and the normalized cross-correlation function. The method is intuitive and easy to use and can be applied on defocused particle images of arbitrary shapes.

General defocusing particle tracking

Rune Barnkob, Christian J. Kähler, and Massimiliano Rossi[*]

A General Defocusing Particle Tracking (GDPT) method is proposed for tracking the three-dimensional motion of particles in Lab-on-a-chip systems based on a set of calibration images and the normalized cross-correlation function. In comparison with other single-camera defocusing particle-tracking techniques, GDPT possesses a series of key advantages: it is applicable to particle images of arbitrary shapes, it is intuitive and easy to use, it can be used without advanced knowledge of optics and velocimetry theory, it is robust against outliers and overlapping particle images, and it requires only equipment which is standard in microfluidic laboratories. We demonstrate the method by tracking the three-dimensional motion of 2-μm spherical particles in a microfluidic channel using three different optical arrangements. The position of the particles was measured with an estimated uncertainty of 0.1 μm in the in-plane direction and 2 μm in the depth direction for a measurement volume of $1510 \times 1270 \times 160\ \mu\text{m}^3$. A ready-to-use GUI implementation of the method can be acquired on `http://www.3D-GDPT.com`.

1 Introduction

Tracking the motion of small particles suspended in a fluid is an important task in microfluidic and lab-on-a-chip technology. For example, suspended particles can be used as passive tracers to measure specific quantities such as the flow velocity,[1,2] the topology of the interface between fluid streams,[3] and the local fluid temperature.[4] In other cases, particle tracking can be used to determine the forces acting directly on the suspended particles e.g. in systems utilizing acoustic radiation forces,[5] dielectric forces,[6] magnetic forces,[7] and inertial forces.[8] An ideal particle tracking method for microfluidic applications should be able to resolve the particle positions in all the three spatial dimensions using a single-camera view, which is the standard in most conventional microscopes. Several techniques fulfilling these requirements are already available e.g. using 3-pinhole mask,[9,10] diffraction ring patterns,[11] astigmatic aberration,[12] and conical-shaped lenses.[13] All methods rely on defocusing of particle images, since the change of particle image shape is related to the depth coordinate, see the sketch in Fig. 1. Here, the depth coordinate is defined along the optical axis of the objective lens. A recent review on this topic can be found in Ref. 14.

In this work, we show that all 3D particle tracking approaches based on defocusing can in principle be evaluated by a single purely empirical method which we refer to as General Defocusing Particle Tracking (GDPT). GDPT requires
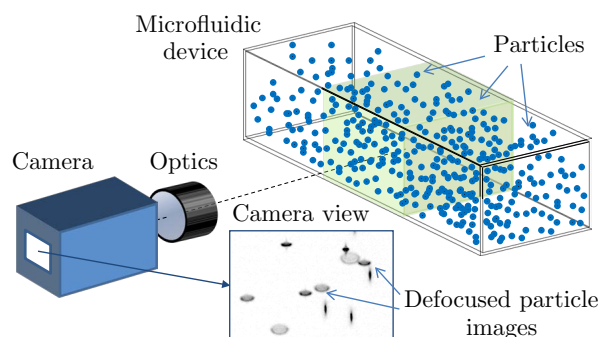
Institute of Fluid Mechanics and Aerodynamics, Bundeswehr University Munich, 85577 Neubiberg, Germany
✉: barnkob@unibw.de; christian.kaehler@unibw.de;
massimiliano.rossi@unibw.de

Fig. 1 Sketch of a single-camera setup for determining the 3D particle positions via defocused particle images, where the particle images change as function of the depth coordinate.

two primary conditions:

1. The optical arrangement must provide defocused particle images with a shape that varies uniquely with the depth coordinate. To fulfill this condition, the tracer particles must have a spherical shape or must be small enough to approximate point sources.

2. It must be possible to obtain a proper calibration image stack, i.e. a set of images reproducing the shape of one defocused particle image for sufficient depth coordinates within the measurement volume.

In comparison with other methods, GDPT possesses a series of key advantages: (*i*) it is applicable to defocused particle images of arbitrary shapes, (*ii*) it requires only equipment which is standard in microfluidic laboratories: micro-
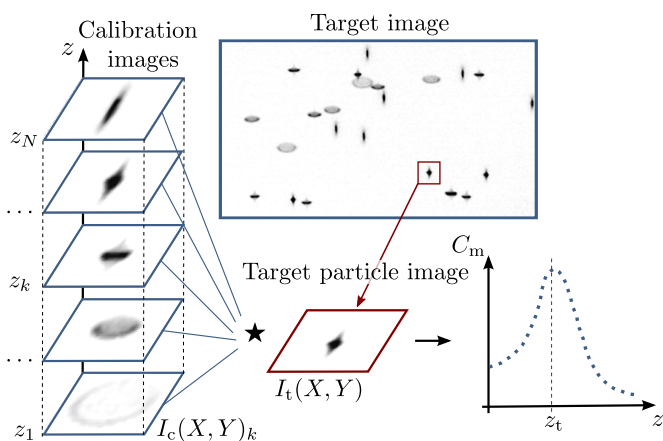
Fig. 2 GDPT working principle: A target particle image I_t is compared to a set of calibration images I_c by use of the normalized cross-correlation (★). The out-of-plane coordinate z_t for the target particle is found where the maximum correlation C_m is highest as a function of the out-of-plane coordinate z.

scope, light source, and camera, (*iii*) it can be used without advanced knowledge of optics or velocimetry theory, (*iv*) it is robust against outliers and overlapping particles, and (*v*) the quality of the evaluation is controlled by a single parameter, namely the quality of a cross-correlation between two images.

2   Method

The GDPT working principle is sketched in Fig. 2. The method relies on a calibration image stack composed by N images, here denoted $I_c(X, Y)_k$, with $k = 1, 2, ..., N$ and where (X, Y) are the in-plane coordinates in image space. Each image in the stack reproduces the defocused image of one particle corresponding to a specific depth coordinate z_k. The z_k-coordinates are equally spaced through a depth $H = z_N - z_1$. H defines the depth of the measurement volume: particles located outside this region will have defocused particle image shapes that are not present in the calibration image stack and therefore they cannot be identified. A straightforward empirical procedure to obtain the calibration image stack is to take pictures of stationary particles (such as sedimented or stuck particles) at different depth positions. This can be done either by moving the particles with a traversing system while keeping the optical settings fixed or by translating the optics (for instance by moving the focus stage of a microscope) while the particles keep their physical positions constant. The two approaches are equivalent and both give the z-coordinates in terms of relative values since the absolute position of the particles is unknown. Specific care must be taken to correctly determine the sign of the z-axis and to account for additional scaling factors (such as the effect of different refractive in-

dices).

At the beginning of each GDPT evaluation, a target image of is searched to identify target particle images at different x and y coordinates using for instance an image segmentation algorithm. Each target particle image, $I_t(X, Y)$, is then compared to the calibration image stack $I_c(X, Y)_k$ to find the best match with one of the k calibration images. To quantitatively rate the similarity between I_t and a calibration image I_c we use the normalized cross-correlation function $c(u, v)$. Following Lewis,[15] it takes the form:

$$c(u, v) = \frac{\sum_{X,Y} \left[I_c(X, Y) - \bar{I}_c \right] \left[I_t(X - u, Y - v) - \bar{I}_t \right]}{\left\{ \sum_{X,Y} \left[I_c(X, Y) - \bar{I}_c \right]^2 \sum_{X,Y} \left[I_t(X - u, Y - v) - \bar{I}_t \right]^2 \right\}^{1/2}},$$

$$(1)$$

where (u, v) are the in-plane coordinates in the correlation space, and $\bar{I}_t$ and $\bar{I}_c$ are the mean intensities of I_t and I_c, respectively. The correlation function $c(u, v)$ will show a maximum peak in the position of best match between I_c and I_t, and the amplitude of this peak, here denoted as C_m, indicates how good the match between the two images is. In particular, C_m takes values between 0 and 1, with $C_m = 1$ indicating a perfect match. Note that the normalized cross-correlation function is not sensitive to fluctuations of the image intensity, for instance due to inhomogeneous light distribution, and takes into account only the similarity in terms of relative intensity. The calibration image stack is then searched until the I_c providing the maximum C_m is identified and the corresponding coordinate z_k will indicate the particle depth position (see Fig. 2). If the maximum C_m is below a certain threshold the particle image is rejected. In this way outliers, for instance caused by overlapping or strongly-distorted particle images, can be reliably filtered out from the analysis. If the particle is accepted, a three-point parabolic fit estimator is applied to refine the z-position with sub-z-scan accuracy. The in-plane position of the particle is simply obtained from the location of the correlation peak in analogy with conventional PIV/PTV analysis.[16] In this case, the $c(u, v)$ calculated with the matched I_c is used and the in-plane position is refined with sub-pixel accuracy using a three-point Gaussian fit estimator. More estimators can be used, however this aspect will not be investigated in this work. At this point the three-dimensional coordinate of the particle is identified and the procedure can be repeated for the following target particle images. Finally, when the particle positions are obtained for target images at different times, the particle trajectories can be connected by means of particle tracking schemes. In this work, a simple nearest-neighbor tracking approach has been used.[17]

The GDPT working principle is completely general and is not restricted to any particular characteristic of the particle
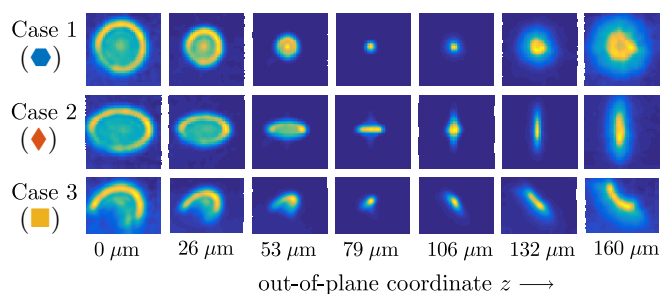
Fig. 3 Selection of experimental particle images as a function of the depth coordinate z from 0 μm to 160 μm for three cases (high pixel intensities in bright colors and low pixel intensities in dark colors). Case 1 (●): Defocused particle images, Case 2 (♦): Astigmatically-aberrated particle images, and Case 3 (■): Astigmatically-aberrated particle images using an odd-shaped aperture mask attached to the back of the objective lens.

Fig. 4 (a-b) Measured depth coordinates z_{meas} (●) and correlation coefficients C_{m} (●) as a function of real depth coordinates z for Case 1 using a 7×7 median filter and number of calibration images (a) $N = 100$ and (b) $N = 10$. (c) Average z-error ϵ_z as a function of number of calibration images N for Case 1 (●), Case 2 (♦), and Case 3 (■). The inset shows ϵ_z for Case 1 as a function of N compared with the use of re-sampling of the calibration images to a fixed number of 100 (empty symbols). (d) Average z-error ϵ_z for Case 1 using $N = 100$ as a function of applied median filter size.

images. The resolution and uncertainty varies case by case and depends on several parameters. Some of them are fixed by the experimental conditions and include the optical properties of the liquid, the particle quality (particle-size distribution, homogenous optical and material properties), and the image quality (signal-to-noise ratio, particle image density, and reproducibility of the defocusing patterns). In this sense, microfluidic applications are ideal as the combination of microscope optics and micrometer-sized particles of low concentration provides in general excellent particle images with clear defocusing patterns. Other parameters can be selected by the user and include the number of calibration images N and type of pre-processing applied to the images (median filter, Gaussian filter, image interpolation, etc.).

3 Application

To access the uncertainty of the method, we measured the Hagen–Poiseuille flow inside a microchannel. The Hagen–Poiseuille flow is commonly used as a benchmark for evaluation of 3D velocimetry methods as it has a well-known flow solution and can be easily realized. The measurements were performed in an isotropically-etched microchannel with a cross-section of width $w = (380 \pm 12)$ μm and height $h = (100 \pm 10)$ μm (Micronit Microfluidics, The Netherlands). The tracer particles were 2.24-μm fluorescent polystyrene spheres (Microparticle GmbH, Germany) suspended in deionized water. In order to examine the sensitivity of the method to different particle image shapes, we used three different optical arrangements referred to as Case 1, Case 2, and Case 3 (Fig. 3). In all cases we looked at defocused particle images taken with a sCMOS camera (16-bit, 2560×2160, PCO GmbH, Germany) mounted on an inverted epi-fluorescent microscope (Axio Observer Z.1, Carl Zeiss AG, Germany)
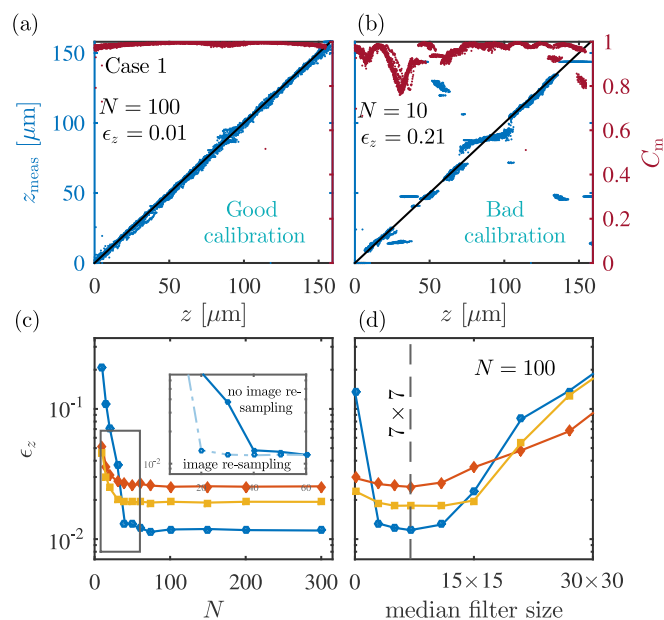
equipped with a double-pulse laser (Litron Lasers, USA) and a $10\times/0.3$ magnification lens. For the Case 2 and 3 an astigmatic aberration was introduced using a cylindrical lens with focal length $f_{\mathrm{cyl}} = 300$ mm in front of the camera sensor. Furthermore, in Case 3 the particle images were distorted by using an odd-shaped aperture mask attached to the back of the objective lens. The entire measurement volume was $1510 \times 1270 \times 160$ μm^3. The signal-to-noise ratio varies significantly along the out-of-plane direction with values from 4 to 147 for Case 1, 5 to 42 for Case 2, and 5 to 62 for Case 3.

Uncertainty analysis. For each case, a set of images at 600 different known depth positions equally spaced across a depth of $H = 160$ μm was taken. These images were used to construct different calibration image stacks using various combinations of N and median filter sizes. Each stack was used to estimate the z-coordinate of all the particles in the 600 images and the results were compared with the real z-coordinate values. In particular, each calibration image stack was created as follows: a subset of N experimental images was extracted from the image set, the selected median filter was applied to them, and for each position a defocused particle image was obtained as an average from 4-5 particles in the image center.
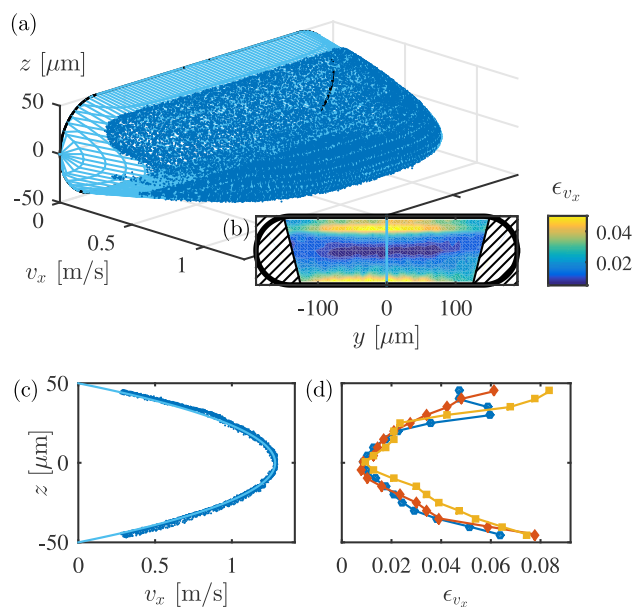
Fig. 5 GDPT measurements of the flow velocity in a microchannel of width $w = 380$ μm and height $h = 100$ μm. (a) Experimental velocity profile $v_x(y,z)$ in the channel cross-section for Case 1 (●) together with the theoretical velocity profile (—) obtained using COMSOL Multiphysics. (b) Colormap of the velocity error ϵ_{v_x} normalized to the maximum velocity. (c) Slice of the experimental velocity profile for -15 μm $< y < 15$ μm (●) and corresponding numerical profile (—). (d) Error ϵ_{v_x} as a function of out-of-plane position z for Case 1 (●), Case 2 (◆), and Case 3 (■).

In Fig. 4(a) and (b) we show the measured depth coordinates z_{meas} (●) and the corresponding correlation values C_{m} (●) as a function of the real depth coordinate z for Case 1 when applying a 7×7 median filter. Panel (a) shows the results obtained using $N = 100$ resulting in a successful measurement of z with an average error of $\epsilon_z = 0.01$ and correlation values C_{m} larger than 0.95. The error is calculated as the sample standard deviation of $z_{\mathrm{meas}} - z$ and normalized to the total depth $H = 160$ μm. Panel (b) shows results obtained using $N = 10$. In this case the number of calibration images in the stack was insufficient to properly determine the depth positions z resulting in strongly biased measurements with low values of C_{m} and an average error of $\epsilon_z = 0.21$. In Fig. 4(c) we plot the average error ϵ_z as a function of the number of calibration images N for the three test cases, Case 1 (●), Case 2 (◆), and Case 3 (■) and when applying a 7×7 median filter. For a number of experimental images $N > 60$ the average error ϵ_z converges to its minimum for all three cases with values of $\epsilon_z = 0.012$ (1.9 μm) for Case 1, $\epsilon_z = 0.025$ (4.0 μm) for Case 2, and $\epsilon_z = 0.019$ (3.0 μm) for Case 3. The minimum N required to achieve the minimal error can be further

reduced down to $N \approx 20$ if image re-sampling is used as shown in the inset for Case 1 (empty symbols). In this case a smoothing spline interpolation was used to re-sample the images to a fixed number of 100 calibration images. Furthermore, in Fig. 4(d) the average error ϵ_z is plotted as a function of the size of the applied median filter for the three cases and $N = 100$. The median filter decreases the error ϵ_z for small filter sizes as it removes salt-and-pepper noise, but as the filter size increases the error increases too due to loss of important features in the particle images resulting in less distinct cross-correlation values. For all three test cases, the median filter size of 7×7 performs the best. The optimal median filter size might of course change for different experimental conditions.

The error ϵ_{xy} in the in-plane position was estimated from the fluctuation of the transverse velocity component in a Hagen-Poiseuille flow (see next section) which is 0 in every position and corresponded to 0.04 μm for Case 1, 0.06 μm for Case 2, and 0.08 μm for Case 3. These values correspond to a displacement uncertainty of approximately 0.1 pixels which is comparable to conventional in-plane PIV or PTV evaluations under real experimental conditions. [14,16]

Flow measurements. The flow in the microchannel was driven by a pressure-controlled system, while 2000 double images were acquired for each test case. The GDPT analysis was performed using $N = 100$, and a median filter of 7×7. All detected particles with $C_{\mathrm{m}} < 0.985$ were rejected resulting in approximately 36,000 valid particles out of 45,000 detected particles for each case. The average evaluation time was 0.1 s/particle using a workstation with an Intel Core 2 Duo Processor E8400 and 8 GB of RAM.

The results are reported in Fig. 5. The experimental velocity profile $v_x(y,z)$ obtained for Case 1 (●) is reported in panel (a) showing a good qualitative agreement with the corresponding numerical solution (—) calculated using COMSOL Multiphysics. This is also evident in panel (c) where a slice of the experimental velocity profile for -15 μm $< y < 15$ μm (●) is plotted showing no outliers and an excellent match with the numerical profile (—). Panel (b) shows the deviation ϵ_{v_x} of the experimental data from the numerical model calculated in terms of sample standard deviation and normalized to the maximum velocity. The hatched areas indicate regions where the measurement was not reliable due to distortions introduced by the curvature of the side walls. The error varies between 1 to 6 % and is larger at the top and bottom. Note that ϵ_{v_x} depends also on ϵ_z (which is one order of magnitude larger than ϵ_{xy}) therefore ϵ_{v_x} will be larger in the regions with larger velocity gradients. Finally, in panel (d) we show the average ϵ_{v_x} for -100 μm $< y < 100$ μm as function of z for Case 1 (●), Case 2 (◆), and Case 3 (■). The results are comparable for the three cases proving that the GDPT method is not sensitive to the particle image shape.

4 Conclusions

We have presented the General Defocusing Particle Tracking (GDPT) method, a single-camera, particle tracking method which is capable of measuring the three-dimensional positions and velocities of particles moving along any trajectory in a transparent fluid. The method relies on a database approach based on a set of calibration images and a normalized cross-correlation analysis to find the correspondence between particle images and calibration images. The method is not restricted to a specific image shape and it can be used to measure any type of particle with an approximate spherical shape, including cells or biological particles, as long as they show a unique defocusing pattern for any depth coordinate. Nonspherical object or deformable cells will result in more complicated defocusing patterns that will increase the uncertainty of the measurement. The method provides an immediate estimation of the depth measurement error as well as easy outlier rejection such as in case of overlapping particle images. To access the uncertainty of the method, we measured a Hagen–Poiseuille flow in a microchannel using three different optical arrangements, obtaining an average error on the depth coordinate in the order of 1-2 % of the measurement volume, and an in-plane error less than 0.1 pixels. The method is simple, reliable, and robust, and is well suited for many Lab-on-a-Chip experiments. A ready-to-use GUI implementation of the method can be acquired on `http://www.3D-GDPT.com`.

References

1 J. Santiago, S. Wereley, C. Meinhart, D. Beebe and R. Adrian, *Experiments in Fluids*, 1998, **25**, 316–319.
2 R. Lindken, M. Rossi, S. Grosse and J. Westerweel, *Lab Chip*, 2009, **9**, 2551–2567.
3 M. Rossi, C. Cierpka, R. Segura and C. J. Kähler, *Measurement, Science & Technology*, 2011, **22**, 105405.
4 R. Segura, M. Rossi, C. Cierpka and C. J. Kähler, *Lab Chip*, 2015, **15**, 660–663.
5 R. Barnkob, P. Augustsson, T. Laurell and H. Bruus, *Lab Chip*, 2010, **10**, 563–570.
6 J. Voldman, *Annu. Rev. Biomed. Eng.*, 2006, **8**, 425–454.
7 N. Pamme, *Lab Chip*, 2006, **6**, 24–38.
8 D. Di Carlo, *Lab Chip*, 2009, **9**, 3038–3046.
9 C. Willert and M. Gharib, *Experiments in Fluids*, 1992, **12**, 353–358.
10 W.-H. Tien, D. Dabiri and J. R. Hove, *Experiments in fluids*, 2014, **55**, 1–14.
11 M. Wu, J. W. Roberts and M. Buckley, *Experiments in Fluids*, 2005, **38**, 461–465.
12 M. Rossi and C. J. Kähler, *Experiments in Fluids*, 2014, **55**, 1–13.
13 C. Snoeyink and S. Wereley, *Experiments in Fluids*, 2013, **54**, 1453.
14 C. Cierpka and C. J. Kähler, *Journal of Visualization*, 2012, **15**, 1–31.
15 J. P. Lewis, *Vision interface*, 1995, **10**, 120–123.
16 M. Raffel, C. E. Willert, S. T. Wereley and J. Kompenhans, *Particle Image Velocimetry*, Springer, New York, 2007.
17 N. Malik, T. Dracos and D. Papantoniou, *Experiments in Fluids*, 1993, **15**, 279–294.